REVIEW OF SCIENTIFIC INSTRUMENTS **84**, 045102 (2013)

A diffracted-beam monochromator for long linear detectors in X-ray diffractometers with Bragg-Brentano parafocusing geometry

N. M. van der Pers, R. W. A. Hendrikx, R. Delhez, and A. J. Böttger
Department of Material Science and Engineering, Delft University of Technology, Delft, The Netherlands

(Received 18 October 2012; accepted 13 March 2013; published online 2 April 2013)

A new diffracted-beam monochromator has been developed for Bragg-Brentano X-ray diffractometers equipped with a linear detector. The monochromator consists of a cone-shaped graphite highly oriented pyrolytic graphite crystal oriented out of the equatorial plane such that the parafocusing geometry is preserved over the whole opening angle of the linear detector. In our standard setup a maximum wavelength discrimination of 3% is achieved with an overall efficiency of 20% and a small decrease in angular resolution of only 0.02 $^{\circ}2\theta$. In principle, an energy resolution as low as 1.5% can be achieved. © *2013 American Institute of Physics*. [http://dx.doi.org/10.1063/1.4798547]

I. INTRODUCTION

The quality of powder diffraction experiments is enhanced by increasing the monochromaticity of the detected radiation, i.e., by avoiding the detection of the background caused by fluorescent radiation of the specimen, and the continuous spectrum and K_β-radiation of a conventional X-ray source. Removing unwanted background can be achieved in several ways either by energy discrimination at the detector or by using a monochromator in the diffracted beam.[1]

In principle, energy discrimination by the detector is the ideal method to remove unwanted background provided that the energy resolution is sufficient. Current energy resolving semi-conductor X-ray detectors reach an energy resolution $\Delta E/E$ of about 3% to 5%, which is sufficient for most purposes. The energy resolution to eliminate K_β lines of conventional X-ray tubes is between 5% and 6%, smaller resolutions could be needed to reduce the effect of fluorescence as, for example, in the steel investigated in this paper.

In this paper a *diffracted* beam monochromator is described that can be used in combination with non-energy discriminating linear detectors and can achieve energy resolutions as low as 1.5%.

Most commonly used powder diffractometers employ the Bragg-Brentano parafocusing geometry to increase the count rate and the angular resolution[2,3] of the diffraction peaks. For point detectors (0D) (in contrast to the position sensitive (1D) detectors discussed in this paper) the monochromator, either of flat or curved type, is simply placed between receiving slit and detector.[4] It then diffracts in the equatorial plane.

By replacing a point detector by a (linear) position sensitive detector, covering a large angular range (typically 5–10 $^{\circ}2\theta$), the measuring time can be decreased by a factor of 50 to 100.[5] This is, in particular, useful for time-resolved experiments or high-throughput data analysis. The highest time resolution is obtained in stationary mode.

For linear detectors with a large opening angle the shape of a diffracted-beam monochromator is complex and no such device is readily available. The main difficulty is to design the curvature such that the parafocusing geometry is preserved over the whole opening angle of the detector. Bragg-Brentano powder diffractometers using flat (graphite) monochromators in the diffracted beam are described in Refs. 6 and 7. Although the amount of fluorescent radiation that can reach the detector is reduced, the usable angular range of the detector is limited to about 5 $^{\circ}2\theta$. In an alternative setup, a single-curved (Johansson-geometry) diffracted-beam monochromator[8] was used. A sufficiently large mosaicity that is homogenously distributed over the monochromator crystal is required to obtain a suitable (and homogeneous) diffracted intensity from the parafocusing geometry. In Ref. 8 the uneven distribution of the mosaicity of the LiF crystal led to inhomogeneity in the intensity of 30%.

In this paper a diffracted-beam graphite monochromator for a linear detector is developed that preserves the Bragg-Brentano focusing geometry. The surface is cone-shaped. Introducing the proposed monochromator in our standard setup (see Sec. III) allows a maximum wavelength discrimination of 3%, with an overall efficiency of 20% and a decrease in angular resolution of only 0.02 $^{\circ}2\theta$. The monochromator shows a uniform intensity response (within 3%) over the whole detector length of 50 mm.

II. DIFFRACTION GEOMETRY AND SHAPE OF THE MONOCHROMATOR

Figure 1(a) shows a schematic drawing of the diffractometer with Bragg-Brentano geometry, the monochromator (diffracting in the axial plan), and a 1D detector. Apart from the divergence and receiving slit systems, the diffracted beam path contains an axial Soller slit and an axial height slit. The Soller slit improves the angular resolution because it limits the axial divergence of the beam to 1° and as will be shown later in combination with the monochromator it also enhances the energy resolution. The axial height slit limits the size of the beam in axial direction.

In this setup a diffracted-beam monochromator can, in principle, be oriented either diffracting in the equatorial plane or diffracting in the axial plane.

In order to diffract the characteristic wavelength $\lambda_{K\alpha}$, the monochromator crystal must be placed at the corresponding Bragg angle, θ_{mono}, in both cases.

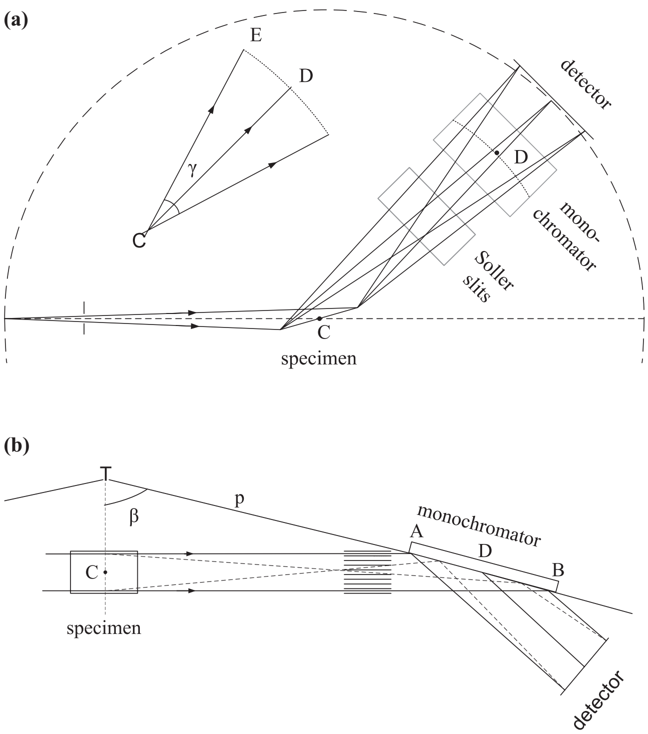

FIG. 1. (a) The diffractometer system, the plane of the drawing coincides with the equatorial plane. The center of the specimen is denoted by C; the monochromator (with the length AB and the center D) is positioned such that diffraction occurs in the axial plane. The inset CDE shows the radius of curvature of the monochromator CD at its center. (b) Axial view of the setup. The cone shape of the monochromator is described by the imaginary axis (TC) and the opening angle β (determined by diffraction angle θ_{mono}). The surface of the monochromator crystal is part of this cone.

By placing the monochromator to diffract in the equatorial plane, a complex (parabola-like) shape is necessary to diffract all rays coming from the center of the specimen and focus them on the detector. Off-center rays will not be focused correctly and reduce the angular resolution and, moreover, also off-center rays with wavelengths different from $\lambda_{K\alpha}$ can diffract and reach the detector. This limits the wavelength discrimination. The combination of a complex shape, large dimension, and limited wavelength discrimination makes this geometry less attractive to apply.

By placing the monochromator to diffract in the axial plane (Fig. 1), both focusing and wavelength discrimination can be achieved as will be discussed next.

In order to maintain the focusing geometry and to enable diffraction of all diffracted beams coming from the center of the specimen and lying within the opening angle (γ) of the detector a curved surface is required. As follows from Fig. 1(a) (inset), the maximum deviation from 90° incident angle (at E) on the crystal equals half the opening angle γ of the detector. This implies that only a very small central area of a perfectly flat monochromator crystal is in diffraction condition. This can, in principle, be solved partly by using a flat crystal with large mosaic spread of which the acceptance angle must be typically several degrees.[6] Such a spread, however, reduces the intensity and angular resolution of the measurement. An ideal monochromator would have a curvature. In the equatorial plane, the crystal should have a curvature with a radius (CD) equal to the distance between the axis through C of the diffractometer and the position on the monochromator crystal (as shown in Fig. 1(a)). This implies that the surface of the crystal must have a variable curvature over its length (AB). The length AB follows from the diffraction angle of the crystal and the effective height of the detector window (see axial plane view Fig. 1(b)). The length of the detector window determines the width of the monochromator.

As the surface of the crystal covers a range of diffractometer radii, it is part of a cone, sharing its imaginary central axis with the diffractometer axis at the center of the specimen.

From the cross section of the cone in Fig. 1(b), it follows that the shape of the monochromator is determined by the radius of curvature r at position p on the monochromator surface by

$$\mathrm{r} = \mathrm{p} \cdot \sin\beta, \tag{1}$$

where β is half of the top angle of the cone, given by $\beta = 90^\circ - \theta_{\mathrm{mono}}$.

The above shape is an approximation because of the finite size of the diffracted beam and the presence of divergence. This implies that some focusing error will occur and that the crystal must possess some mosaic spread to accept the beam divergence, i.e., the optimal mosaic spread of the monochromator crystal is to be about the divergence of the beam (typically 1°). The simplification of the shape does not affect the overall wavelength discrimination, which is determined by the divergence in the axial plane (as will be discussed next) and not by the divergence in the equatorial plane.

Wavelength discrimination can be achieved as follows: The axial view of Fig. 2 illustrates that the Soller slit system positioned before the monochromator (i) limits the axial divergence and (ii) determines the acceptance angle of all the radiation (including fluorescence) coming from the sample.

The axial divergence is determined by the total acceptance angle (α_{s}) of the Soller slit, defined as

$$\alpha_{\mathrm{s}} = 2\arctan(\mathrm{w}/\mathrm{L}), \tag{2}$$

where L is the length of the Soller slit and w is the spacing between the individual foils.

The wavelength (λ) or energy (E) resolution at a reflection angle is, in general, related to the acceptance angle $\Delta\theta$ in

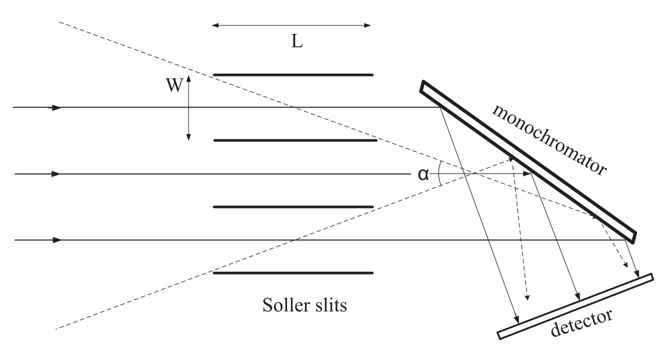

FIG. 2. Sketch of the axial view of the Soller slit system in front of the monochromator, the axial divergence of the beam is limited by the acceptance angle α_{s} of the Soller slit, α_{s} is determined by the length (L) of the foils and the spacing (w) between the individual foils. For clarity the number of foils of the Soller slit is strongly reduced.

radians of the object in the diffracted beam and Bragg's law by[9]

$$\Delta\lambda/\lambda = \Delta E/E = \Delta\theta/\tan(\theta_{\mathrm{Bragg}}). \quad (3)$$

For a Soller slit, with acceptance angle α_s given in radians, placed between the specimen and the monochromator crystal, it thus holds for the wavelength (energy) resolution that

$$\Delta\lambda/\lambda = \Delta E/E = \alpha_s/\tan(\theta_{\mathrm{mono}}). \quad (4)$$

It is easily seen that the intensity distribution of the beam transmitted by the Soller slit has, approximately, the shape of a triangle with an opening angle α_s. The effect of the Soller slit on the wavelength discrimination will be illustrated and quantified in more detail in Sec. IV.

At the monochromator crystal each wavelength λ_i in the beam diffracts according to its corresponding Bragg angle $\theta_{i,\mathrm{mono}}$. Thus, the range of the possible diffraction angles is determined by the mosaic spread of the monochromator crystal as

$$\Delta\lambda_i/\lambda_i = \omega/\tan(\theta_{i,\,\mathrm{mono}}) \quad (5)$$

with ω being the mosaic spread of the crystal in radians; see for definition and discussions on mosaicity Ref. 10. Consequently, besides radiation of wavelength $\lambda_{K\alpha}$, a part of the radiation of other wavelengths can reach the monochromator and diffract (and be detected).

III. EXPERIMENTAL

The monochromator is designed for Co K_α radiation and used in a Bruker-AXS D8 Advance diffractometer. The instrument is equipped with a Co long fine focus 0.4 mm × 12 mm, X-ray source with 6° take-off angle. The detector is a Vantec-1 with an active area of 50 mm × 16 mm (length x height) and an energy resolution <25% (according to Bruker Spec Sheet XRD17). With the radius of the diffractometer set at 550 mm the detector covers an angular range of 10° 2θ. For all measurements the same slit systems are used, i.e., in the incoming beam a divergence slit system is used so that the divergence is 1° and in the diffracted beam a scatter slit and a receiving slit are placed. The receiving slits are taken such that the full length (50 mm) of the detector is used. The Soller slit and the axial height slit, placed directly before the detector, are varied for specific experiments as is indicated in the text. In the standard setup a Soller slit with acceptance angle $\alpha_s = 2.6°$ and an axial height slit of 8 mm is used.

The general principles are applicable to other instruments and wavelengths.

A. Construction of the monochromator

A Highly Oriented Pyrolytic Graphite (HOPG) sheet has been chosen as the monochromator material. This material shows high reflectivity and can be easily shaped.[10–12] The graphite crystal sheet was obtained from Optigraph GmbH, Berlin, Germany, with the following specifications: AGraphZ quality with a mosaic spread of 0.4°, plane of diffraction {002} with inter-planar spacing of 0.33354 nm, and thickness of 300 μm.

The shape of the monochromator is determined by the substrate. To enable shaping and mounting the crystal as smooth as possible without glue, an optically flat quartz substrate is used. The substrate has been cut computer-controlled in the shape of a cone according to Eq. (1) with a tolerance on the radius of ±0.1 mm, a shape accuracy of 10 μm, and a surface roughness of 50 nm. The overall surface roughness and shape of the substrate were according to the specifications as confirmed by light interferometry. The mosaic spread of the mounted HOPG surface was investigated by rocking curve measurements of the {002} reflection in two perpendicular directions (parallel and normal to AB). The FWHM in the central region of the monochromator is about 0.55° and increases somewhat near the edges.

For CoK_α radiation, the corresponding Bragg angle of the monochromator crystal is $\theta_{\mathrm{mono}} = 15.55°$. By using a HOPG sheet thickness of 300 μm it is effectively infinitely thick for CoK_α radiation.

B. Performance of the monochromator

The performance of the monochromator is evaluated by comparing all measurement with the monochromator in place (without K_β-filter) with a reference measurement with only a K_β-filter in the diffracted beam. All the measurements are performed with an incident beam divergence of 1° and the full opening of the Vantec detector. Unless indicated otherwise, the diffracted beam path contains an assembly with several slits: receiving scatter, axial Soller ($\alpha_s = 2.6°$), receiving, and axial height slit (8 mm).

The intensity response (homogeneity check) of the monochromator–detector assembly is investigated by measuring the scattered intensity from a Perspex plate in stationary mode. This specimen produces a relatively high and uniform CoK_α background in the measured 2θ-range (around 113° 2θ). The uniformity is within 3%.

The efficiency, i.e., overall intensity loss, is estimated from the net area intensity ratio of the {311} reflection of an Al_2O_3 (corundum) bulk powder sample in scanning mode. Figure 3 shows a measurement of the {311} reflection of Al_2O_3 bulk powder sample in scanning mode with

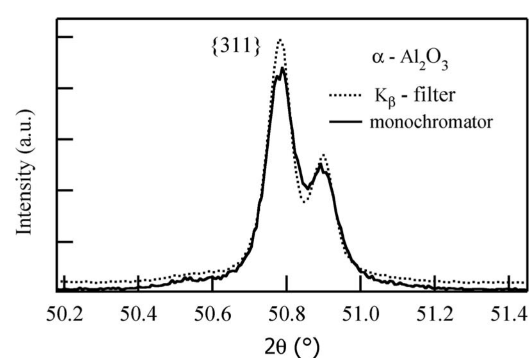

FIG. 3. The efficiency of the diffracted-beam monochromator is estimated from the intensity of the Kα1/Kα2 doublet of the {311} reflection of α-Al_2O_3 (corundum). The intensity reduction by the monochromator is about a factor of 5. The data obtained with the monochromator are scaled to the net peak intensity of the {311} reflection obtained with K_β filter.

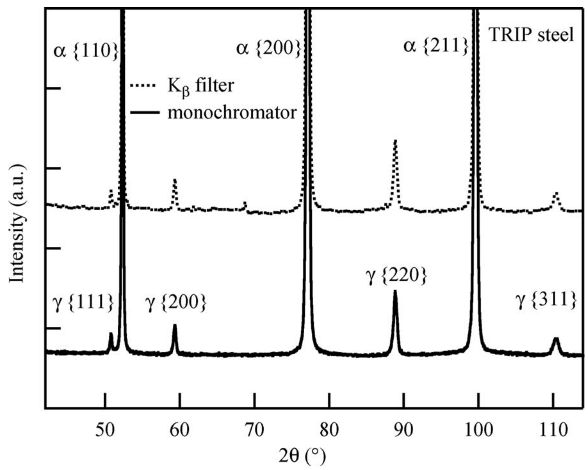

FIG. 4. Diffraction patterns of the two-phased TRIP steel with monochromator and with K_β-filter (without monochromator), Soller slit: $\alpha_s = 2.6°$. The reflections of ferrite (α) and austenite (γ) are indexed. The monochromator strongly suppresses the background that is mainly caused by the fluorescence of Mn and Fe in the steel. The data obtained with the monochromator are scaled to the net peak intensity of the {110} reflection obtained with K_β filter.

monochromator and without monochromator but with K_β-filter. From the net area intensity ratio it follows that the intensity reduction by the monochromator is a factor of 4.7.

Next, the effect of the monochromator on the wavelength discrimination, i.e., on the suppression of the background and the reduction of the contribution of the K_β radiation to the measurements, is demonstrated. In Fig. 4 the diffraction pattern of a TRIP steel specimen (composition see Table I) in scanning mode is shown. In addition to the Fe fluorescence, the fluorescence of Mn, in this sample, gives rise to a high overall background level. The ratio of the net area of the (weak) austenite {200} reflection at around 60° 2θ and its background is 0.067 for the measurement with monochromator and 0.027 for the reference measurement with K_β-filter (no monochromator).

The contribution of the K_β radiation to the diffraction pattern has been investigated using a LaB_6 SRM660a[13,14] powder specimen (Fig. 5). The inset shows detail of the measurement of the LaB_6 powder in scanning mode. From the strong LaB_6 {110} reflection, the net area ratio of the CoK_β and CoK_α component is 0.2% for the measurement with monochromator and about 2% for the reference measurement with K_β-filter.

The data from the measurement on LaB_6 (see Fig. 5) is also used to evaluate the resolution in 2θ. The FWHM (width at half maximum intensity) values for the $CoK_{\alpha1}$ component of all the reflections are given in Fig. 6. The measurements with monochromator show a small and almost constant amount (~0.02 °2θ) of extra peak broadening in respect to the reference. This is an indication that the focusing geometry of the diffracted beam is largely maintained.

TABLE I. Main elements (>0.15 wt. %) in the TRIP steel specimen in wt. % as determined by XRF analysis.

Fe	Mn	Al	Si	Mg	P	Cu	Zn	Other
94.80	1.57	1.15	1.11	0.34	0.22	0.19	0.19	0.43

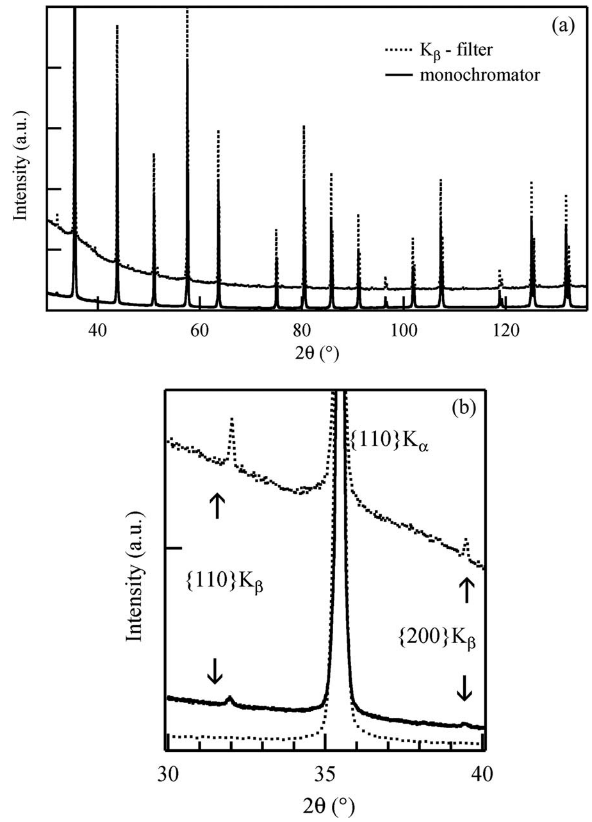

FIG. 5. (a) Diffraction pattern of LaB_6 with monochromator and with K_β-filter (without monochromator), Soller slit: $\alpha_s = 2.6°$. The monochromator largely suppresses the low angle background that is mainly caused by air scatter. (b) Suppression of the unwanted {110} K_β and {200} K_β reflections for different opening angles of the Soller slits, from top to bottom, $\alpha_s = 2.6°$ K_β-filter (no monochromator), $\alpha_s = 2.6°$ with monochromator, $\alpha_s = 1.5°$ with monochromator. The data obtained with the monochromator are scaled to the net peak intensity of the {110} reflection obtained with K_β filter.

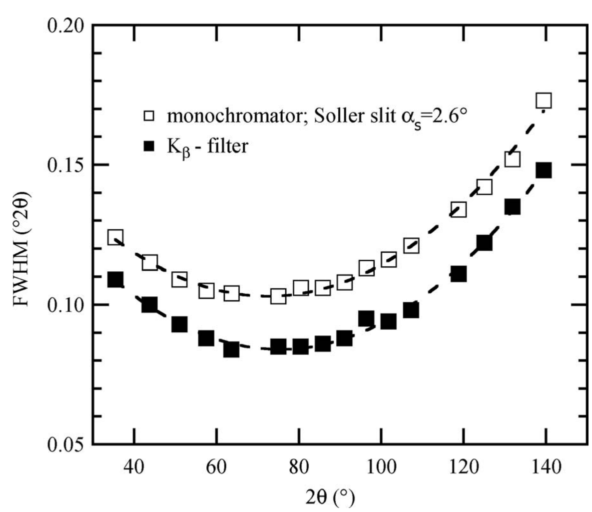

FIG. 6. The effect of the monochromator on the angular resolution is illustrated by the FWHM of the individual LaB_6 reflections.

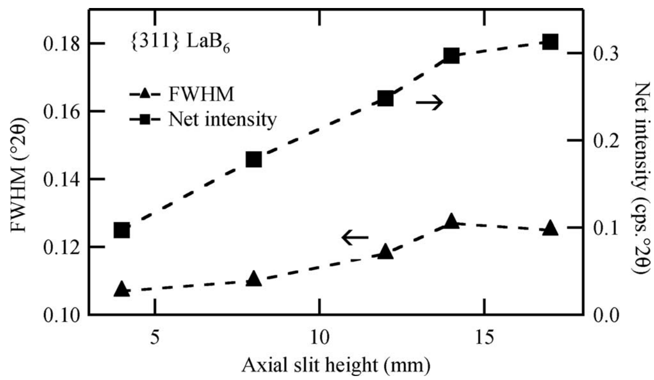

FIG. 7. The FWHM and the net intensity of the {311} LaB_6 reflection as a function of the axial height slit size. By increasing the slit size the net intensity increases significantly whereas the angular resolution is only slightly reduced.

IV. DISCUSSION

The homogeneity of the monochromator–detector response is comparable with the one without monochromator indicating that the mosaicity over the monochromator is sufficiently uniform. The experiments show that the intensity loss caused by the monochromator is about a factor of 5. This intensity loss is somewhat larger than that expected for a graphite monochromator but may be explained by the somewhat higher effective mosaic spread of the mounted monochromator (0.55°) compared to the specifications of the HOPG (0.4°). A larger effective mosaic spread reduces the reflectivity.[14] Further optimization of the setup is obtained by using a larger (than 8 mm) axial height slit. The effect of the size of the axial height slit has been evaluated using the LaB_6 {311}. From Fig. 7 it is clear that higher intensities are observed with only a slight loss in resolution when increasing the slit width. The performance is optimal with an axial height slit of about 12 mm. A significant net intensity increase of about a factor of 1.5 is achieved with only a small reduction in the resolution (0.01 °2θ) with respect to the 8 mm axial height slit.

The effect of the monochromator on the reduction of the background is obvious for both TRIP steel and LaB_6 although the cause of the background is quite different. In the case of LaB_6, the background is mainly caused by air scatter of the primary beam and not by fluorescence of the material. The net peak to background ratio near the {110} reflection (see Fig. 5) is improved by a factor of 5 with respect to the reference measurement with only K_β filter. Due to the axial orientation of the monochromator, direct entrance of this air scatter in the detector window is prevented. This setup results in a considerably smaller overall background level in respect to the reference also for negligibly fluorescent material.

For the TRIP steel the background is mainly from fluorescence of Fe and Mn, using the monochromator reduces it significantly. The net peak intensity to background ratio increases about a factor of 2.5 but part of the fluorescence is still detected. As mentioned earlier in Sec. II, the wavelength discrimination is affected by the acceptance angle of the Soller slit. Using the value of $\alpha_S = 2.6°$ and $\lambda(CoK_\alpha) = 0.179$ nm, Eq. (4) gives for the wavelength resolution $\Delta\lambda = 0.030$ nm,

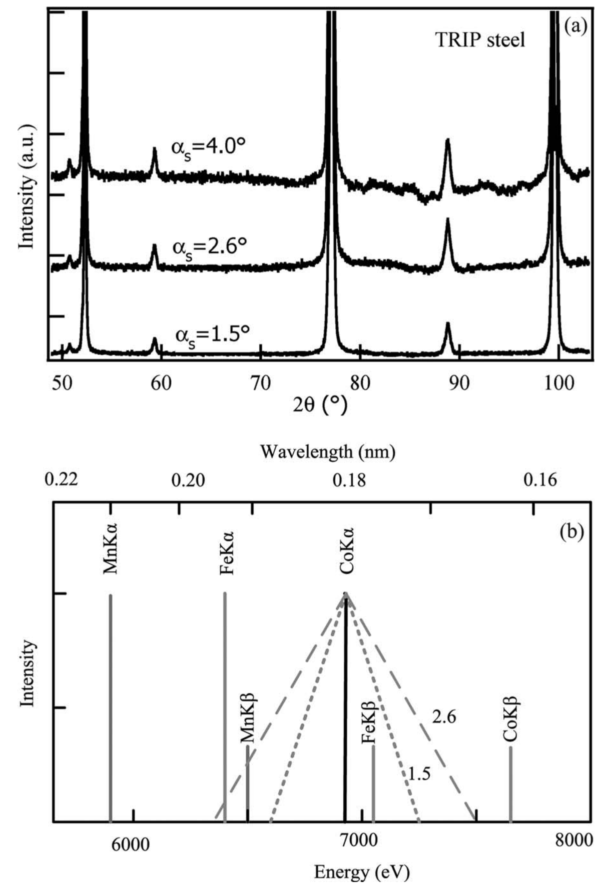

FIG. 8. (a) Effect of the Soller slits acceptance angle on the background suppression of the TRIP steel specimen. Axial height slit of 8 mm is used. (b) Schematic of the diffracted and fluorescent radiation and the transmitted intensity profiles for Soller slits with acceptance angle 1.5° and 2.6°. Note: Intensities are not to scale.

i.e., ±0.015 nm around CoK_α. The corresponding energy resolution is about 560 eV FWHM or 8%. In the case of the TRIP steel the main contributions to the background come from K_β-radiation from Co, Fe, and Mn, and K_α-radiation from Fe and Mn. Both MnK_α ($\lambda = 0.210$ nm) and CoK_β ($\lambda = 0.162$ nm) are outside the wavelength acceptance range, but FeK_β ($\lambda = 0.176$ nm), MnK_β ($\lambda = 0.191$ nm), and FeK_α ($\lambda = 0.194$ nm) are within (see Fig. 8(b)) and thus contribute to the residual background in Fig. 4.

The effect of the Soller slit acceptance angle on the background intensity is illustrated in Fig. 8(a) for measurements of the TRIP steel sample performed with Soller slits with acceptance angles of 4°, 2.6°, and 1.5°, respectively. Clearly, a smaller acceptance angle of the Soller slit leads to a large improvement of the net peak intensity to background ratio, for the ferrite {110} reflection this was from 0.22 (no Soller slit) to 0.87 ($\alpha_S = 2.6°$ Soller slit) and 2.2 ($\alpha_S = 1.5°$ Soller slit). This latter case corresponds to an energy resolution of about 325 eV FWHM (4.5%). In Fig. 8(b) the diffracted and fluorescent radiation and the transmitted intensity profiles for Soller slits are schematically given for two acceptance angles of the Soller slit. With the last optimization step using the smallest Soller slit also the contribution of the CoK_β is removed (see inset Fig. 5). The better energy resolution by using smaller Soller slits reduces the overall efficiency of the setup, for an acceptance angle of 1.5° the intensity is reduced with a factor of 9. This loss can be reduced by a factor of 2 by increasing the axial height slit at the cost of some resolution (see Fig. 7). Thus, an efficiency of about 20% is achieved with a small additional loss of resolution of 0.01 °2θ with respect to the standard setup.

Even for the standard setup with $\alpha_S = 2.6°$ the energy resolution is better than the newest currently available position sensitive detector (of length 14 mm) based on silicon strip detector technology that has an energy resolution of 600 eV.[15] By using a Soller slit with a smaller acceptance angle, the wavelength discrimination can be improved. Ideally, the acceptance angle of the Soller slit should be the same as the effective mosaic spread of the monochromator crystal, i.e., in this case $\alpha_S = 0.55°$ (cf. Eqs. (3)–(5)). This will improve the wavelength discrimination resulting in a maximal energy resolution of 120 eV FWHM or about 1.5%.

V. CONCLUSIONS

The cone-shaped diffracted-beam monochromator developed for a linear detector maintains the Bragg-Brentano parafocusing geometry over the total length of the detector. The monochromator achieves excellent wavelength discrimination without important losses in efficiency and resolution. The diffractometer equipped with the monochromator yields diffraction patterns with optimal peak to background ratio even for strongly fluorescent material and a negligible K_β contribution. The wavelength and energy discrimination of the monochromator-Soller slit assembly can be optimized up to 1.5%, which is better than the best solid-state detectors (0D) currently available.

[1] M. J. Fransen, Adv. X-Ray Anal. **47**, 224 (2004).
[2] V. K. Pecharsky and P. Y. Zavalij, *Fundamentals of Powder Diffraction and Structural Characterization of Materials* (Springer Science and Business Media, LLC, 2009), p. 128.
[3] J. Brentano, Arch. Sci. Phys. Nat. **44**, 66 (1917).
[4] H. P. Klug and L. E. Alexander, *X-Ray Diffraction Procedures* (Wiley, New York, 1954), pp. 211–218.
[5] H. P. Klug and L. E. Alexander, *X-ray Diffraction Procedures for Polycrystalline and Amorphous Materials*, 2nd ed. (John Wiley & Sons, New York, 1974), pp. 354–356.
[6] M. A. Beno and G. S. Knapp, Rev. Sci. Instrum. **64**, 2201 (1993).
[7] S. Megtert, D. Dallé, and D. Petermann, Mater. Sci. Forum **79–82**, 377 (1991).
[8] M. A. Beno, G. S. Knapp, and G. Jennings, Rev. Sci. Instrum. **63**, 4134 (1992).
[9] B. D. Cullity and S. R. Stock, *Elements of X-Ray diffraction*, 3rd ed. (Prentice-Hall, New Jersey, 2001).
[10] A. K. Freund, A. Munkholm, and S. Brennan, Proc. SPIE **2856**, 68 (1996).
[11] H. Legall, H. Stiel, P. V. Nickles, A. A. Bjeoumikhov, N. Langhoff, M. Haschke, V. A. Arkadiev, and R. Wedell, Proc. SPIE **5918**, 591802 (2005).
[12] M. Sanchez del Rio, M. Gambaccini, G. Pareschi, A. Taibi, A. Tuffanelli, and A. Freund, Proc. SPIE **3448**, 246 (1998).
[13] SRM 660a, *Lanthanum Hexaboride Powder Line Position and Line Shape Standard for Powder Diffraction*, (National Institute of Standards and Technology, U.S. Department of Commerce, Gaithersburg, MD, 2000).
[14] J. L. Lawrence, Acta Cryst. **A38**, 859 (1982).
[15] W. Dabrowski, J. Fink, T. Fiutowski, H.-G. Krane, and P. Wiacek, J. Instrum. **7**, P03002 (2012).